Krawtchouk Moment Invariant And Gaussian ARTMAP Neural Network: A Combination Techniques For Image Classification

[1]Shahrul Nizam Yaakob and [1]Puteh Saad,

[1]Artificial Intelligence and Software Engineering Research Lab
School of Computer and Communication Engineering
Northern University College of Engineering (KUKUM)
Blok A, Kompleks Pusat Pengajian, Jalan Kangar-Arau,
02600 Jejawi, Perlis.
ysnizam@gmail.com, puteh@kukum.edu.my

ABSTRACT

The main objective of this research is to develop a practical system for binary image classification using Krawtchouk Moment Invariant (KMI) as the feature extraction technique while Gaussian ARTMAP (GAM) is adopted for classification task. Fundamentally, KMI is introduced by P.T. Yap back in 2003 based on the discrete orthogonal function which is invariant to position, scale and rotation factors. This technique is used to extract the global shape feature of binary images. As a comparison we also applied two other types of features extraction methods that are Geometric Moment Invariant (GMI) and Legendre Moment Invariant (LMI). In doing so, 20 dissimilar types of insect with totally of 240 images have been used for classification purposes. Furthermore, we have applied k-folds cross validation technique in order to seek the reliability of the techniques used. In this research, we found that KMI generated the highest classification rate of GAM which is about 99% compare to GMI (91%) and LMI (97%). The high share numbers for KMI, GMI and LMI demonstrated that GAM neural networks is well efficient technique for classification. In addition, the combination of GAM and KMI methods is one of the brilliant concepts in developing a fully practical system for binary image classification based on the global shape features.

Keywords: Krawtchouck Moment Invariant (KMI), Gaussian ARTMAP (GAM).

1. INTRODUCTION

Classification process is one of the important elements in an image recognition process. In order to identify an image, there are several processes that required for attention by of developers. Basically, three essential stages are needed; image preprocessing, feature extraction and image classification. However in this paper, we will concentrate on the two last processes which are the features extraction and classification. For the feature extraction stage the moment invariant technique is used. Thus, three different types of moment will be examined that are GMI, LMI and KMI. Moment invariant has been widely used over the years as features extraction technique for recognition and classification in many areas of image analysis [R.Mukundan *et al*. 2001, S.Paschalakis *et al*. 1999]. This method is successfully adopted along with other techniques in order to produce an efficient image recognition system. From our observation, most of the work conducted that used moment methods are based on the binary images especially for the optical character recognition (OCR) application. For example M.Sarfraz *et al*. (2003) applied the GMI to extract the shape information of Arabic text for recognition purposes. However, some used grey-scaled images as demonstrated by S.Paschalakis *et al*. (1999). It is found that, moment invariant is one of the commonly used methods to extract the shape of character images. Since character existed in various forms, thus the moment technique is a suitable technique to be used. Since it preserves the invariant properties of images against translation, position and rotation.

Normally, classifiers techniques such as neural networks linear discriminate analyst are used to evaluate the performance of each the moment technique studied. Moment technique that shows the highest classification is chosen as the feature extraction in the image classification application. J. Haddania et al. (2001) used Radial Basis Function (RBF) to classify feature vectors of human faces extraction using Pseudo Zernike Moment Invariant (PZMI), ZMI and LMI. He found that, PZMI produces the highest classification rate. A.Saradha *et al*. (2001) also have demonstrated that LMI is the best techniques compare to ZMI and GMI because it produced the highest recognition rate by using Linear Discriminate Analysis (LDA) classifiers. However, we also found that, KMI are not commonly in used since all of this technique is new. However, B.Bayraktar *et al*. (2005) had applied KMI for features extraction of handwritten characters. They also have demonstrated the percent changes between feature vectors of original image and it variation. Furthermore, they have shown that, KMI have better shape description capability compared to Normalize Zernike Moment Invariant (NZMI), Zernike Moment Invariant (ZMI) and GMI.

However, it is also found that, GAM neural network is not often applied in many applications. However J.R.Wiliamson (1996) had demonstrated that GAM achieved higher classification rate of 95.3% while Fuzzy ARTMAP (FAM) produced 91.73% in letter image recognition problems. D. Muchoney *et al*. (2001) also shows that, GAM produced 83% of classification rate while FAM generates 79% in classifying of remote sensing data. Therefore, this has convinced us to apply GAM neural network for the classification of insect images. The organizations of this paper are as follows. Section 2 describe the fundamental equation for all moment techniques applied that are GMI, LMI and KMI. In Section 3 contains an important concept of GAM neural network as classifiers. Section 4 contains the details of each process and stages involved in this research. Meanwhile, Section 5 and Section 6 discuss the experimental result and the conclusion.

2. FEATURES EXTRACTION TECHNIQUE

In this research, moment invariant based techniques are used to extract the shape properties of the binary images. This is also known as *Silhouette* moments [R.Mukundan *et al*. 1998] where it refers to moments calculated from binary images. The pixels on the object region are assigned a value one (1) and others are assigned as zero (0). Based on these methods, each image is represented by a set of features vector.

I. Geometric Moment Invariant (GMI)

In 1961, Hu introduced the moment invariant based on the theory of algebraic function. He derived a set of moment invariants, which are translation, scaling and rotation independent. This method is also known as Geometric Moment Invariant (GMI). The $(p+q)^{th}$ geometric moment for p, q = 0, 1, 2, 3…… are define in (1). Where $h(x,y)$ is an image of the size N X M. To make these moments invariant to translation, central moments (2) is derived based on (1). Where $\bar{x} = m_{10} \div m_{00}$ $\bar{y} = m_{01} \div m_{00}$. In order to produce the invariant properties with scaling factor, the central moment than be normalized using (3). The seven (7) functions of central moments that are invariant to rotational and scale differences are shown in (4).

$$m_{pq} = \sum_{x=1}^{N} \sum_{y=1}^{M} x^p y^q h(x,y) \tag{1}$$

$$\mu_{pq} = \sum_{x=1}^{N} \sum_{y=1}^{M} (x-\bar{x})^p (y-\bar{y})^q h(x,y) \tag{2}$$

$$\eta_{pq} = \frac{\mu_{pq}}{\mu_{00}^{\frac{p+q+2}{2}}} \tag{3}$$

$$\phi_1 = (\eta_{20} + \eta_{02})$$

$$\phi_2 = (\eta_{20} - \eta_{02})^2 + 4\,\eta_{11}^2$$

$$\phi_3 = (\eta_{30} - 3\,\eta_{12})^2 + (3\,\eta_{21} - \eta_{03})^2$$

$$\phi_4 = (\eta_{30} + \eta_{12})^2 + (\eta_{21} + \eta_{03})^2$$

$$\phi_5 = (\eta_{30} - 3\,\eta_{12})(\eta_{30} + \eta_{12})[(\eta_{30} + \eta_{12})^2 - 3(\eta_{21} + \eta_{03})^2] + (3\,\eta_{21} + \eta_{03})(\eta_{21} + \eta_{03})[3(\eta_{30} + \eta_{12})^2 - (\eta_{12} + \eta_{03})^2]$$

$$\phi_6 = (\eta_{20} - \eta_{02})[(\eta_{30} + \eta_{12})^2 - (\eta_{21} + \eta_{03})^2] + 4\,\eta_{11}(\eta_{30} + \eta_{12})(\eta_{21} + \eta_{03})$$

$$\phi_7 = (3\,\eta_{12} - \eta_{03})(\eta_{30} + \eta_{12})[(\eta_{30} + \eta_{12}) - 3(\eta_{21} + \eta_{03})] - (\eta_{30} - 3\,\eta_{12})(\eta_{12} + \eta_{03})[3(\eta_{30} + \eta_{12})^2 - (\eta_{21} + \eta_{03})^2] \tag{4}$$

II. Legendre Moment Invariant (LMI)

The Legendre moment was introduced by Teague (1980) which is produced based on Legendre polynomials. The Legendre moments of order (p+q) can be expressed in terms of geometric moments as shown in eq. (5) whereas in eq. (6) $|x|\leq 1$ and (n-k) is even. The purpose of v_{pq} is to provide TMI equation invariant against translation, scaling and rotation factors.

$$L_{pq} = \frac{(2p+1)(2q+1)}{4} \sum_{i=0}^{p} \sum_{j=0}^{q} a_{pi} a_{qj} m_{ij} \tag{5}$$

$$a_{pi} = P_n(x) = \sum_{k=0}^{n} (-1)^{(n-k)/2} \frac{1}{2^n} \frac{(n+k)!\, x^k}{\left(\frac{n-k}{2}\right)!\left(\frac{n+k}{2}\right)!\, k!} \tag{6}$$

$$v_{pq} = M_{00}^{-\gamma} \sum_{x=1}^{N} \sum_{y=1}^{N} [(x-\bar{x})\cos\phi + (y-\bar{y})\sin\phi]^p \times [(y-\bar{y})\cos\phi - (x-\bar{x})\sin\phi]^q f(x,y) \tag{7}$$

Where:

$$\gamma = \frac{n+m}{2} + 1 \tag{8}$$

$$\phi = 0.5 \tan^{-1} \frac{2\mu_{11}}{\mu_{20} - \mu_{02}} \tag{9}$$

III. Krawtchouk Moment Invariant (KMI)

Krawtchouk moment invariants were derived by P.T Yap et al. (2003) using the concept of Krawtchouk polynomial function with the implementations of linear combinations of Geometric Moment. The (p+q) order of Krawtchouk moment is given by (10). In order to make Krawtchouk Moment is invariant to scaling and rotation factors, he used the concept of linear combination with GMI which shown in equation (14).

$$\tilde{Q}_{nm} = \Omega_{nm} \sum_{i=0}^{n} \sum_{j=0}^{m} a_{i,n,p1} a_{j,m,p2} \tilde{v}_{ij} \tag{10}$$

$$\Omega_{nm} = \left[\rho(n; p_1, N-1)\rho(n; p_2, N-1)\right]^{-0.5} \tag{11}$$

$$\rho(n; p, N) = (-1)^n \left(\frac{1-p}{p}\right)^n \frac{n!}{(-N)_n} \tag{12}$$

$$\sum_{k=0}^{n} a_{k,,n,p} x^k = \sum_{k=0}^{n} \frac{(-n)_k (-x)_k}{(-N)_k} \times \frac{p^{-k}}{k!} \tag{13}$$

$$\tilde{v}_{ij} = \sum_{p=0}^{i} \sum_{q=0}^{j} \binom{i}{p}\binom{j}{q} \left(\frac{N^2}{2}\right)^{\frac{p+q}{2}+1} \left(\frac{N}{2}\right)^{i+j-p-q} v_{pq} \tag{14}$$

$$\binom{x}{y} = \frac{x!}{(x-y)!x!} \tag{15}$$

3. GAUSSIAN ARTMAP (GAM)

In 1996, J.R.Wiliamson introduced Gaussian ARTMAP (GAM) based on Fuzzy ARTMAP neural network architecture and separable Gaussian distribution. Basically, GAM incorporates of four basic combinations that are pair of Gaussian ART modules ART_a and ART_b, Associate learning network, internal controller module and a mapfield F^{ab}. The GAM general structure can be illustrated as in Figure 2. Where I_a is the input vector of *ARTa* and I_b is the input vector of *ARTb*. Figure 5 illustrates the architecture of Gaussian ART module where they are no need for complement coding of input vector. Each category J in F_2 layer will be presented by three different parameters which are count n_j, min μ_J and standard deviation σ_J. Therefore, each Gaussian ART category will consist of $2M+1$ components to represent M-dimensional input, $I=(I_1,\ldots\ldots,I_M)$. Figure 4 illustrates the architecture of mapfield and connection with the F_2 of *ARTa* and F_2 of *ARTb*. w^{ab}_{ji} characterize the weight vectors that connect the F_2 of *ARTa* with the mapfield. Where k define the number of categories in the mapfield. Fundamentally, the number for both categories in mapfield and F_2 of *ARTb* are same. In addition, the output vector of mapfield is defined as X^{ab}.

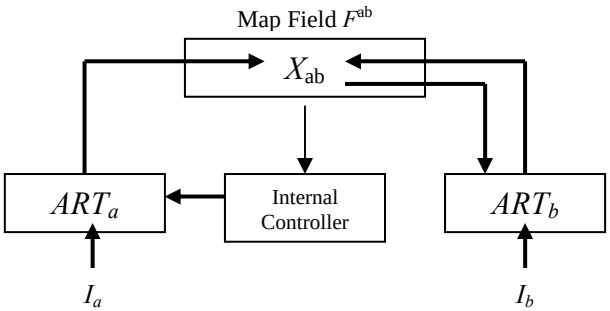

Figure 2: Fuzzy ARTMAP general architecture.

During the training phase, the input vector I and its desired output vector are presented to *ARTa* and *ARTb* respectively. *ARTa* and *ARTb* modules classify the input pattern and desired output vector into categories, then the input to the mapfield module use the vigilance parameter whether *ARTa* categories corresponds to *ARTb* categories. Fundamentally, Gaussian ART performance is determined by the value of gamma parameter γ. The first step involved in the learning phase is the computation of category choice in Gaussian ART module. The category choice function (CCF) $g_j(I)$ for each input vector I and F_2 node j can be define using equation (16). The next step is to find the maximum value among $g_j(I)$ or called the competitive process using equation (17).

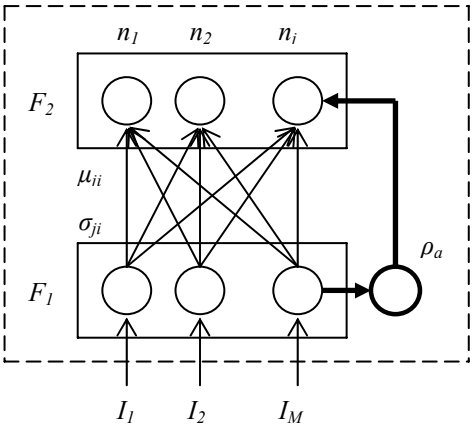

Figure 3: Gaussian ART module.

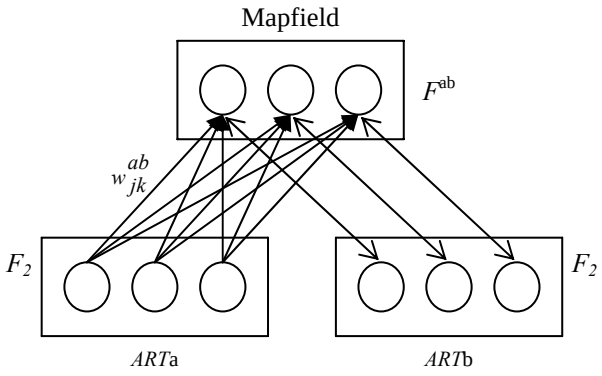

Figure 4: The position of Mapfield between two Gaussian ART.

$$g_j(I) = -\frac{1}{2}\sum_{i=1}^{M}\left(\frac{\mu_{ji} - I_i}{\sigma_{ji}}\right)^2 - \log\left(\prod_{i=1}^{M}\sigma_{ji}\right) + \log P(j) \tag{16}$$

$$g_j(I)_{winner} = \max\left\{g_j(I) : j = 1.....m\right\} \tag{17}$$

$$g'_j(I) = -\frac{1}{2}\sum_{i=1}^{M}\left(\frac{\mu_{ji} - I_i}{\sigma_{ji}}\right)^2 \tag{18}$$

$$g'_j(I) \geq \rho \tag{19}$$

Only one node (or category) with the highest of $g_j(I)$ will be selected and continue with category resonance. Resonance occurs if the category match function (CMF) as shown in equation (18) of the chosen category meets the vigilance criterion given in equation (19). When the J^{th} category is chosen, y_J=1 and y_j=0 for $J \neq j$. If the $g'_J(I)$ doesn't meet the criterion requirement therefore, the value of the choice function g_J is set to zero (0) for the duration of the input presentation and a new index j then chosen using equation (17). Until now, all the procedures happen simultaneously for both Gaussian *ARTa* and *ARTb*. Next stage is to find the value of X^{ab}. If the J^{th} of F^a_2 node is active and K^{th} of F^b_2 is active therefore, the value of X^{ab} can be computed using equation (20). When both *ARTa* and *ARTb* are active as well as $X^{ab} \neq 0$, then the weight vector between F^a_2 layer and mapfield F^{ab} can be initialized using the equation (21). Furthermore, the value of count parameter and the min of the winner node then is updated using equation (22) and (23) respectively. While the standard deviation value for the particular node is updated using equation (24). If X^{ab}=0 then the vigilance parameter ρ of *ARTa* will be increased slightly higher and thus, the competitive process start again and a new category had to be find until the condition satisfy with the desired output vector using equation (19). If there is no winner, thus a new node will be created and the value of input vectors is assigned as the min. While the counter n_j is set to one and the standard deviation is set as the gamma parameter value.

$$X^{ab} = y^b \wedge w_j^{ab} \tag{20}$$

$$w_j^{ab} = \begin{cases} 1 & j = J; k = K \\ 0 & otherwise \end{cases} \tag{21}$$

$$n_j(t) = n_j(t-1) + 1 \tag{22}$$

$$\mu_{ji}(t) = \left(1 - n_j^{-1}(t)\right)\mu_{ji}(t-1) + n_j^{-1}(t)I(t) \tag{23}$$

For $n_j > 1$:

$$\sigma_{ji}(t) = \sqrt{\left(1 - n_j^{-1}(t)\right)\sigma_{ji}^2(t-1) + n_j^{-1}(t)\left(\mu_{ji}(t) - I_i\right)^2} \tag{24}$$

For $n_j = 1$;

$$\sigma_{ji}(t) = \gamma$$

For the testing stage the best category *K* of GAM mapfield is chosen using equation (26) whereas m refers to the number of categories available in mapfield. This is done by summing the activations of all categories in F^a_2 layer that map to each prediction of category *k* of mapfield as illustrated in equation (25).

$$H_k = \sum_{j=1}^{J} \exp\left(g_j(I)\right) \tag{25}$$

$$H_K = \max\left(H_k : k = 1.....m\right) \tag{26}$$

4. EXPERIMENTAL WORKS

In this research, we used two dimensional binary images that represent the global shape of insect. For more generalize, we applied 20 different types of insect images which every insect would have 12 more images with different scale and rotation factors. Figure 6 illustrates an example of the binary insect images and its variation counterparts used in this work. There are four dissimilar types of rotation factors been chosen namely 5°, 15°, 20° and 45°. While for the scaling factors, we choose the value randomly that are 0.5X, 0.75X, 1.3X and 1.5X. In order to get more variation, there are three images for every insect that are created under the influence of both scaling and rotation factors. This is done by adding up 5° with 1.5X, 15° with 1.3X and 20° with 0.75X. Figure 6 illustrates all the examples of binary images under the influence of scaling and rotation factors, while Table 5.1 shows the relation between the images and its orientation. Therefore, in this research we have 240 binary insect images used for classification purposes. To make the further work easier, we have to standardize the image dimension to 800X800 pixels.

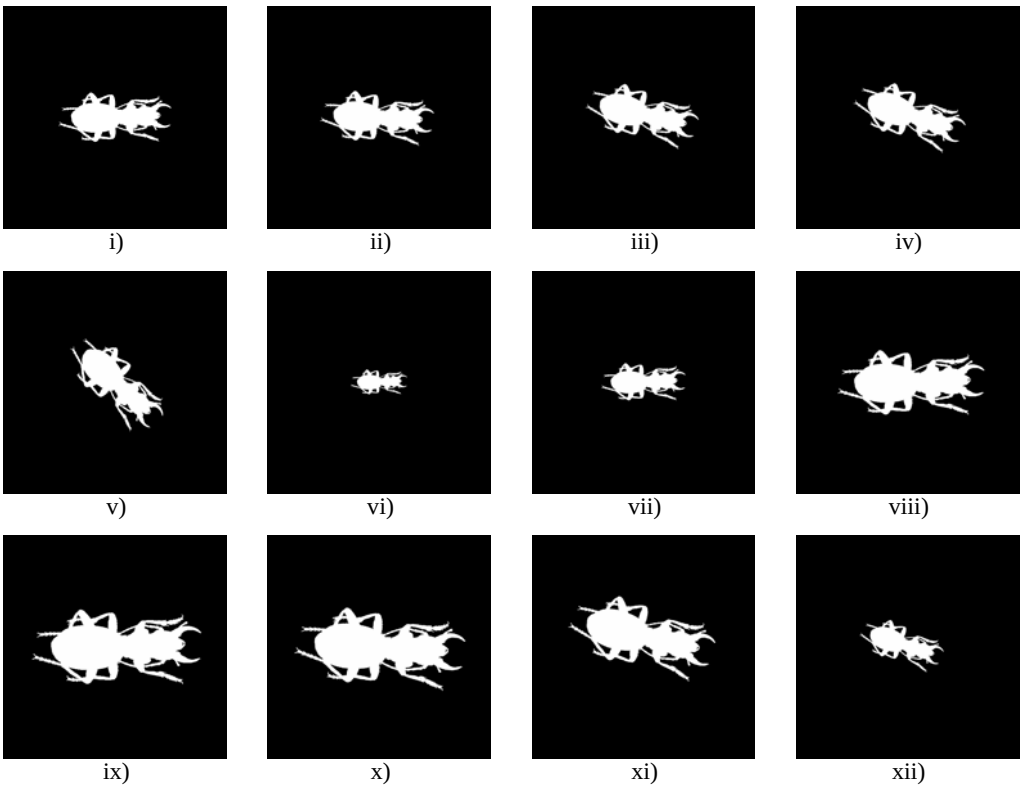

Figure 5: An example of binary insect (*Anthia sexguttata - carabidae*) images with its variations.

Table 5.1: Types of variation for insect images.

i	: original image
ii	: the image is rotated to 5°
iii	: the image is rotated to 15°
iv	: the image is rotated to 20°
v	: the image is rotated to 45°
vi	: the image is reduced to half of its original size
vii	: the image is reduced to 0.7X of its original size
viii	: the image is enlarged 1.3 X its original size
ix	: the image is enlarged 1.5 X its original size
x	: the image is rotated to 5° and enlarged 1.5 X
xi	: the image is rotated to 15° and enlarged 1.3 X
xii	: the image is rotated to 20° and enlarged 0.75 X

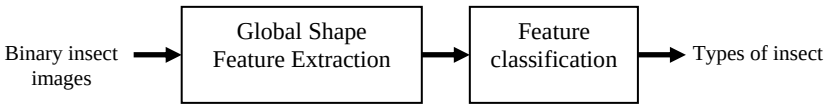

Figure 6: The overall process for binary image classification of this work.

Figure 5 illustrates the overall process involved for binary insect classification of this work. Its start with the extraction of global shape feature of the binary images. This was done by using the fundamental concept of moment invariant and for these paper three different types of moment techniques namely KMI, GMI and LMI have been used. At the end of this stage, each image will be presented with one feature vector F^a_m (also known as pattern) with six

dimensions. The details of each dimension of the feature vector produced by GMI, LMI and KMI techniques are shown in equation (5.1) to (5.3). As we can see from those equations, in this research we tried to apply the lower order moment for all the feature extraction techniques. On the classification stage (see Figure 5) the entire feature vectors than will be classified using the supervised GAM neural network.

In order to find the generalization performance of GAM in conjunction with features vector produced by different type of feature extraction techniques studies, the method of *k*-fold cross validations adopted. In this work the available data *G* is split into *k* mutually exclusive subsets, designated as G_1, G_2, G_3….G_k of equal size. The classifier is than trained and tested *k* – times. In this research the value of *k* is set to 4. The cross validation estimate is defined as the number of correct classification divided by the number of data points in the set *G*. The percentage of correct classification (PCC_k) is given by (27) and the number of correct classification (NCC_k) is given by (28). $\sigma(x,y)_t$=1 if the testing vector true, otherwise $\sigma(x,y)_t$=0 and *n* refer to the number of data (or feature vectors) being tested. Hence, in this work *n* is equal to 60 (240 divided by *k*=4).

$$PCC_k = 100\frac{1}{G}\sum_{k=1}^{4} NCC_k \tag{27}$$

$$NCC_k = \sum_{t=1}^{n} \sigma(x,y)_t \tag{28}$$

5. RESULTS AND DISCUSSION

Table 1 to Table 3 describe the original feature vectors produced from three different moment invariant techniques applied for shape features extraction from the binary images. The feature vectors are extracted from all images illustrated in Figure 6. As we can see from all the tables, different moment method will generated a dissimilar value of feature vectors for the same image. Also note that, as the order of the moment increase, we found that, the feature vector produced are less sensitive to the invariant characteristic. This situation can clearly be seen especially for GMI. From moment invariant point of view, this dilemma also known as the *discreatization error* (For more details of this problem please refer to [Liao, S.X. & Pawlak, M. (1996).]). Furthermore, the scaling factor of 0.5X generated feature vector that have the smallest similarity of its values measure up to the original feature vector compare to other scaling and rotation factors. This circumstance occurred for all moment invariant technique applied. We found that as the image of the insect becomes smaller compare to its original image, the value of feature vector produced is less invariant from the others. This problem is also known as *spatial quantization error*.

Table 1: An example of feature vectors produced GMI.

	φ1	φ2	φ3	φ4	φ5	φ5
Original	0.2784481920	0.0388318342	0.0006253833	0.0004165021	-0.0012484687	0.0000820737
5	0.2733892349	0.0369562509	0.0004606425	0.0003174091	-0.0009478201	0.0000610091
15	0.2733593175	0.0369651386	0.0004586030	0.0003153795	-0.0008935388	0.0000606330
20	0.2733215327	0.0369445458	0.0004624830	0.0003187096	-0.0008585123	0.0000612559
45	0.2726478890	0.0367247689	0.0004591467	0.0003133759	-0.0004922466	0.0000600514
05X	0.2670572999	0.0348149428	0.0002980891	0.0002199658	-0.0006593890	0.0000410420
075X	0.2710044109	0.0361457325	0.0003981565	0.0002793426	-0.0008374502	0.0000531062
13X	0.2732643666	0.0369031535	0.0004598620	0.0003190227	-0.0009566097	0.0000612742
15X	0.2731541399	0.0369170068	0.0004519380	0.0003108400	-0.0009318729	0.0000597207
5+15X	0.2716480159	0.0363603674	0.0004127359	0.0002885215	-0.0008619570	0.0000550126
15+13X	0.2713798030	0.0362586114	0.0003999121	0.0002838950	-0.0008017203	0.0000540429
20+075X	0.2677762542	0.0350036438	0.0003264525	0.0002325225	-0.0006269402	0.0000435021

Table 2: An example of feature vectors produced by LMI.

	L20	L02	L21	L12	L30	L03
Original	0.0406951229	0.2377530691	-0.0034179944	-0.0010428513	0.0008131802	0.0430952603
5	0.0405745742	0.2328146608	-0.0027099999	-0.0007862913	0.0008418148	0.0374372107
15	0.0405480580	0.2328112594	-0.0027049609	-0.0010287211	0.0008583899	0.0373207446
20	0.0405559463	0.2327655865	-0.0027032846	-0.0010178529	0.0008611411	0.0375066041
45	0.0405054065	0.2321424825	-0.0027518903	-0.0010970813	0.0009110374	0.0372389921
05X	0.0402348361	0.2268224639	-0.0017757143	-0.0010982100	0.0008307643	0.0308461361
075X	0.0404420501	0.2305623607	-0.0023915916	-0.0010164009	0.0008386522	0.0350210951
13X	0.0405812157	0.2326831509	-0.0026654974	-0.0007251194	0.0008162951	0.0374978623
15X	0.0405080754	0.2326460645	-0.0026868947	-0.0009758776	0.0008409493	0.0370520606
5+15X	0.0404820347	0.2311659812	-0.0024616659	-0.0009720536	0.0008490055	0.0356123584
15+13X	0.0404814311	0.2308983720	-0.0023384666	-0.0006951510	0.0008667908	0.0352549339
20+075X	0.0403418233	0.2274344309	-0.0020601366	-0.0011715585	0.0008921712	0.0318705996

Table 3: An example of feature vectors produced by KMI.

	Q20	Q02	Q21	Q12	Q30	Q03
Original	195648588.7	267035816.8	21301124316.2	25339416043.3	-5923179887.3	-5923492942.4
5	195604918.1	265246803.5	21298659978.4	25238216360.2	-5923180099.3	-5923451050.4
15	195595312.2	265245571.3	21298116631.6	25238144587.6	-5923180222.0	-5923450188.1
20	195598169.8	265229025.6	21298278297.6	25237208712.8	-5923180242.4	-5923451564.2
45	195579861.0	265003296.7	21297242180.8	25224438883.4	-5923180611.8	-5923449582.8
05X	195481842.8	263076039.3	21291705767.5	25115416732.3	-5923180017.5	-5923402250.3
075X	195556909.2	264430873.7	21295946907.2	25192058434.2	-5923180075.9	-5923433161.6
13X	195607324.1	265199162.1	21298796462.1	25235521876.3	-5923179910.4	-5923451499.5
15X	195580827.9	265185726.9	21297297429.4	25234759729.2	-5923180092.9	-5923448198.8
5+15X	195571394.2	264649544.3	21296765705.3	25204428693.5	-5923180152.6	-5923437539.3
15+13X	195571175.6	264552598.8	21296754387.4	25198946992.2	-5923180284.2	-5923434892.9
20+075X	195520600.5	263297733.7	21293895808.3	25127957031.4	-5923180472.2	-5923409835.4

The main purpose of this work is to classify the binary images. In order to do so, we adopted supervised GAM neural network as the classifier. However, GAM requires one parameter to be initialized which refers to the gamma parameter γ. Other parameters are mathematically obtained from the data patterns that were trained to GAM. Basically, different types of moment generate various dataset thus the value of gamma is also dissimilar from one dataset to another. Table 4 illustrates all gamma values adopted for every types of moment dataset in cross validation process. Table 5 demonstrates the cross validation result for GAM. Notice that, the GAM classification result for the feature vectors generated from all moment techniques applied is definitely high (above 90% of correct classification). However KMI produced the highest classification with 99.58% are correct compare to GMI (90.42%) and LMI (98.75%). In addition, from the Table 5 also we can notice that KMI generated the lowest number of category. These reveal that, KMI can save the computational memory used since its only generated small number of category in GAM architecture especially compared to GMI. This is a great advantage if we have a huge number of feature vectors (e.g. more than 10000) to be classify by GAM.

Table 4
The value of Gamma applied for GA cross validation

	k	No test data	ρA	NodeA	*NCC*
GMI	1	60	-50.57	50	54
	2	60	-33.87	51	59
	3	60	-79.74	34	53
	4	60	-32.52	59	51
				PCC	90.42
LMI	1	60	-32.44	27	60
	2	60	-23.31	29	59
	3	60	-78.19	20	58
	4	60	-22.13	32	60
				PCC	98.75
KMI	1	60	-28.61	29	60
	2	60	-28.24	28	60
	3	60	-28.02	21	60
	4	60	-29.22	29	59
				PCC	99.58

Table 5
Cross Validation result for GA.

	Gamma,γ
GMI	0.0001
LMI	0.001
KMI	$1X10^9$

Note: *NCC* = number of correct classification *PCC* = Percentage of correct classification

6. CONCLUSION

We have demonstrated the techniques that can be applied in order to classify the binary images. In this paper we have shown on how the moment invariant methods can be used to extract the global shapes features of binary insect images while the supervised GAM neural network can be adopted as the classifier. We also found that KMI had produced the feature vectors that are more invariant against scaling and rotation factors. In addition, KMI also generated the highest classification rate of GAM compare to GMI and LMI. We also realized that this research is still at an early stage and need to be further developed in order to achieve more practical and robust system for insect classification. However, this work has opened few venues for future work such other method also can be used for global shape features extraction technique such as Fourier descriptors (FD). For example Qing Chen *et al*. (2003) used FD technique for optical character recognition (OCR). Therefore, it is an interesting research to be done especially using FD compared to moment invariant for feature extraction technique of binary insect images. Besides a hybrid feature extraction also is an interesting method to be examined in the future. Saradha, A. *et al*. (2005) have demonstrated that by combining FD and ZMI, they manage to produce higher classification rate of face images using LDA as classifier compare to LMI, GMI and ZMI. Even other types of supervised ARTMAP neural networks also can be used to classify insect images such as Ellipsoid ARTMAP (AE), Hypersphere ARTMAP (HA) and Fully Self Organizing MAP (FOSART). For example Anagnostopoulos, G.C *et al* (2001) have demonstrated that Ellipsoid ARTMAP (EA) neural network perform better compared to the conventional GAM in solving the Circle in a Square problem. Furthermore, there are two main factors which reduce the invariant capability of each types of moment invariant technique which are *spatial quantization* and *discreatization error*. However, different types of moment possess dissimilar percentage error causing by this two elements.

7. REFERENCES

[1] Anagnostopoulos, G.C. & Georgiopoulos, M. (2001). Ellipsoid ART and ARTMAP for incremental clustering and classification. International Joint Conference on Neural Networks, 2001. Proceedings IJCNN '01, Volume: 2, Pages: 1221 – 1226.

[2] Bayraktar B. (2005). Feature extraction for cellular systems in the context of high-content screening (HCS) using computational image analysis and pattern recognition tools. Purdue University Cytometry Laboratories.

[3] Haddadnia, J., Faez, K. & Moallem, P. (2001). Neural network based face recognition with moment invariants. Proceedings 2001 International conference on Image Processing, Volume: 1, Pages: 1018 – 1021.

[4] Liao, S.X. & Pawlak, M. (1996). On image analysis by moments. IEEE Transactions on Pattern Analysis and Machine Intelligence, Volume 18, Issue 3, Page: 254 – 266.

[5] Ming-Kuei Hu. (1962). Visual pattern recognition by Moment invariants, IEEE Transactions on information Theory, Volume: 8, Issue: 2, Pages: 179 – 187.

[6] Muchoney, D. & Williamson, J. (2001, Sept.). A Gaussian adaptive resonance theory neural network classification algorithm applied to supervised land cover mapping using multitemporal vegetation index data. IEEE Transactions on Geoscience and Remote Sensing, Volume: 39, Issue: 9, Pages: 1969 – 1977

[7] Mukundan, R. & Ramakrishnan, K.R. (1998). *Moment Functions in Image Analysis Theory and Applications*. World Scientific.

[8] Mukundan, R., Ong, S.H. & Lee, P.A. (2001). Image analysis by Tchebichef moments, IEEE Transactions on Image Processing, Volume 10, Issue 9, Page(s):1357 – 1364.

[9] Puteh B.Saad. (2004). Feature Extraction of Trademark Images Using Geometric Invariant Moment and Zernike Moment-A Comparison , *Chiang Mai Journal of Science* , 20 July 2004.

[10] Qing Chen, Emil Petriu & Xiaoli Yang (2004). A comparative study of Fourier descriptors and Hu's seven moment invariants for image recognition. Canadian Conference on Electrical and Computer Engineering, 2004, Volume: 1, Pages: 103 - 106 Vol.1

[11] Qing Chen & Petriu, E.M. (2003). Optical character recognition for model-based object recognition applications. Proceedings the 2nd IEEE International Workshop on Haptic, Audio and Visual Environments and Their Applications, 2003. HAVE 2003. Pages: 77 – 82.

[12] Paschalakis,S. & Lee.P. (1999). Pattern Recognition in grey level images using moment based invariant features. Seventh International Conference on Image Processing And Its Applications, Volume: 1, Pages: 245 – 249.

[13] Saradha, A. & Annadurai, S. (2005). A Hybrid Feature Extraction Approach for Face Recognition Systems. The International Congress for Global Science and Technology 2005 (ICGST 05). Volume: 5, Pages: 23-30.

[14] Sarfraz, M, Nawaz, S.N. & Al-Khuraidly, A. (2003). Offline Arabic text recognition system; Proceedings. 2003 International Conference on Geometric Modeling and Graphics, Pages: 30 – 35.

[15] Teague M.R. (1980). Image analysis via the general theory of moments. Journal of the Optical Society of America, volume 70, No. 8, pp. 920-930.

[16] Wiliamson, J.R. (1996). Gaussian ARTMAP: A neural network for fast incremental learning of noisy multidimensional maps. *Neural Networks*, vol. 9, no.5, pp. 881-897.

[17] Yap, P.T., Paramesran, R. & Seng-Huat Ong (2003). Image analysis by Krawtchouk moments, IEEE Transactions on Image Processing, Volume: 12, Issue: 11, Pages: 1367 – 1377.